


Article

Label-Free Electrochemical Sensing Using Glassy Carbon Electrodes Modified with Multiwalled-Carbon Nanotubes Non-Covalently Functionalized with Human Immunoglobulin G

Michael López Mujica^{1,†}, Alejandro Tamborelli^{1,2,†}, Pablo Dalmaso^{2,*}  and Gustavo Rivas^{1,*}

¹ INFIQC, CONICET-UNC, Departamento de Fisicoquímica, Facultad de Ciencias Químicas, Universidad Nacional de Córdoba, Ciudad Universitaria, Córdoba 5000, Argentina; mlopezmujica@unc.edu.ar (M.L.M.); alejandrotamborelli@gmail.com (A.T.)

² CIQA, CONICET, Departamento de Ingeniería Química, Facultad Regional Córdoba, Universidad Tecnológica Nacional, Maestro López esq. Cruz Roja Argentina, Córdoba 5016, Argentina

* Correspondence: pdalmaso@frc.utn.edu.ar or p-dalmaso@hotmail.com (P.D.); gustavo.rivas@unc.edu.ar (G.R.)

† These authors contributed equally to this work.

Abstract: This work reports new analytical applications of glassy carbon electrodes (GCE) modified with a nanohybrid obtained by non-covalent functionalization of multi-walled carbon nanotubes (MWCNTs) with human immunoglobulin G (IgG) (GCE/MWCNT-IgG). We report the label-free and non-amplified breast cancer 1 gen (BRCA1) biosensing based on the facilitated adsorption of the DNA probe at the nanohybrid modified GCE and the impedimetric detection of the hybridization event in the presence of the redox marker benzoquinone/hydroquinone. The resulting genosensor made the fast, highly selective, and sensitive quantification of BRCA1 gene possible, with a linear range between 1.0 fM and 10.0 nM, a sensitivity of $(3.0 \pm 0.1) \times 10^2 \Omega \text{ M}^{-1}$ ($R^2 = 0.9990$), a detection limit of 0.3 fM, and excellent discrimination of fully non-complementary and mismatch DNA sequences. The detection of BRCA1 in enriched samples of diluted human blood serum showed a recovery percentage of 94.6%. Another interesting analytical application of MWCNT-IgG-modified GCE based on the catalytic activity of the exfoliated MWCNTs is also reported for the simultaneous quantification of dopamine and uric acid in the presence of ascorbic acid, with detection limits at submicromolar levels for both compounds.

Keywords: BRCA1 gene; impedimetric biosensor; biomarker; carbon nanotubes; human immunoglobulin G; breast cancer; dopamine; uric acid; ascorbic acid



Citation: Mujica, M.L.; Tamborelli, A.; Dalmaso, P.; Rivas, G. Label-Free Electrochemical Sensing Using Glassy Carbon Electrodes Modified with Multiwalled-Carbon Nanotubes Non-Covalently Functionalized with Human Immunoglobulin G.

Chemosensors **2024**, *12*, 4. <https://doi.org/10.3390/chemosensors12010004>

Academic Editor: Andrea Ponzoni

Received: 10 November 2023

Revised: 22 December 2023

Accepted: 25 December 2023

Published: 28 December 2023



Copyright: © 2023 by the authors. Licensee MDPI, Basel, Switzerland. This article is an open access article distributed under the terms and conditions of the Creative Commons Attribution (CC BY) license (<https://creativecommons.org/licenses/by/4.0/>).

1. Introduction

The advent of nanomaterials has been revolutionary for the field of electrochemical biosensors due to their unique optical, electrical and magnetic properties [1]. In this regard, carbon nanostructures such as graphene, graphene oxide, carbon nanoparticles, carbon nanodots, carbon nanofibers, and carbon nanotubes (CNTs) have attracted considerable attention in the last years [2,3]. Multi-walled carbon nanotubes (MWCNTs) present a unique porous structure, large surface area, important chemical stability, high mechanical strength, strong corrosion resistance, and facilitated electron transfer [4]. Since the first report about the use of CNTs for the preparation of electrochemical sensors, there has been an exponential increment in the number of publications focused on CNTs-based electrochemical sensors due to their highly improved analytical performance. In fact, the role of CNTs was crucial for the development of novel architectures able to support the biorecognition elements and new schemes for the transduction of the bioaffinity event [5,6], demonstrating that the combination of the known advantages of electrochemical sensors [7,8] with the unique properties of CNTs allowed the successful quantification of different biomarkers of clinical relevance [9–11].

Due to the strong van der Waals interaction, the CNTs are aggregated, forming bundles in water that limit further sensing applications. Therefore, a functionalization step is mandatory to exfoliate them [12,13]. In particular, the non-covalent functionalization with biomolecules is demonstrated to be a very powerful strategy, not only to exfoliate the nanostructures but also to provide them with different biorecognition properties depending on the biomolecule (enzymes, nucleic acids, and glyco-biomolecules) [6,14–20]. Recently, we have reported the advantages of the non-covalent functionalization of MWCNTs with human immunoglobulin G (IgG), a biomolecule that not only exfoliates the nanostructures but also maintains the immunorecognition properties, even after the drastic treatment used to prepare the nanohybrid [21]. The partial denaturation of IgG facilitates the non-covalently functionalization of MWCNTs due to the stronger interaction of phenylalanine and tyrosine residues with MWCNTs via π - π stacking and van der Waals forces [22]. López Mujica et al. [21] proposed two interesting analytical applications of GCE/MWCNT-IgG, one original immunosensor strategy for the development of immunosensors based on the use of the immunoglobulin that supports the MWCNTs as biorecognition layer, without needing of an extra step for the covalent attachment of the antibody, and one an electrochemical sensor for the quantification of uric acid taking advantage of the catalytic activity of the exfoliated nanostructures.

The present work reports two new analytical applications of the MWCNT-IgG nanohybrid: (i) the label-free and non-amplified impedimetric quantification of the BRCA1 gene without the requirement of an oriented immobilization of the DNA probe, and (ii) the simultaneous quantification of dopamine (Do) and uric acid (UA) in the presence of ascorbic acid (AA), taking advantage of both, the catalytic activity of the exfoliated MWCNTs and the charge of the protein that supports the CNTs.

The human BRCA1 (Breast CAncer 1) gen is located on the long (q) arm of chromosome 17 at position 21 (17q21), and is related to a protein that acts as a tumor suppressor and repairs damaged DNA [23,24]. The mutations of this gene have been associated with the risk of developing breast and ovarian cancer [25]. Due to its role in genetic predisposition to cancer, the BRCA1 gen has become a significant biomarker for the early detection and prognosis of cancer [26,27]. Currently, there are robust techniques such as sequence analysis and multiplex ligation-dependent probe amplification (MLPA), that are used for mutation detection. However, these techniques are expensive and require well-trained personnel [28]. In this sense, the electrochemical biosensors represent an interesting analytical tool for competitive BRCA1 quantification. Several biosensors based on the use of polymers, modified carbon nanomaterials and/or antimonene, with or without amplification schemes, have been reported in the last years [29–40].

Do and UA are important biomarkers that coexist in biological fluids. Do is a catecholaminergic neurotransmitter that plays a central role in the transmission of information in the central nervous system, accompanied by the release of hormones during physiological processes [41,42]. The abnormal Do level can be associated with schizophrenia, Parkinson's disease, and Alzheimer's disease, among others [43,44]. UA is the primary end product of purine metabolism and is present mainly in urine and blood. Abnormal UA concentrations can be related to different pathologies like cardiovascular diseases, hypertension, and gout [45–47]. In addition, UA is an important natural antioxidant that demonstrates a relevant neuroprotective role in diseases related to oxidative stress. In fact, a low serum UA concentration has been associated with an increased risk of developing neurodegenerative diseases [48]. Thus, the efficient quantification of Do and UA is of great importance for human and animal health monitoring [49,50]. Electrochemical sensors have been widely used for the quantification of both analytes due to their widely known advantages [51–55]. However, since Do and UA are oxidized at similar potentials [56], their simultaneous quantification at common electrodes is not possible, and new strategies are highly required to discriminate both oxidation processes.

In the following sections, we discuss the adsorption and electrooxidation of BRCA1-DNA probe at glassy carbon electrodes (GCEs) modified with multi-walled carbon nan-

otubes non-covalently functionalized with IgG (GCE/MWCNT-IgG), the optimization of the hybridization conditions for BRCA1 impedimetric biosensing, and the simultaneous and selective voltammetric determination of Do and UA in the presence of AA.

2. Materials and Methods

2.1. Reagents

MWCNTs (outer diameter: 6–13 nm, length: 2.5–20 μm , purity > 98%), human serum immunoglobulin G (IgG) (catalog number I4506), bovine serum albumin (BSA), hydroquinone (HQ), benzoquinone (BQ), dopamine (Do), and uric acid (UA) were provided by Sigma-Aldrich (St. Louis, MO, USA). Ascorbic acid (AA) was obtained from Anedra (Troncos del Talar, Buenos Aires, Argentina). All reagents used were analytical grade. DNA sequences, purchased from Invitrogen (Waltham, MA, USA), are the following:

Target (BRCA1): 5'-GAA CAA AAG GAA GAA AAT C-3'

DNA probe (DNAP): 5'-GAT TTT CTT CCT TTT GTT C-3'

Non-complementary sequence (NC): 5'-CTA ACC CCA CCG ACC TCG G-3'

Mismatch (Mi): 5'-GAA GAA GAA GAA GAA GAA C-3'

The enriched samples of human blood serum samples were obtained by adding the BRCA1 gene to reconstituted samples of serum (Wiener lab., Rosario, Santa Fe, Argentina) diluted 1/100 with 0.050 M phosphate buffer pH 7.40 + 0.500 M NaCl.

Ultrapure water (resistivity = 18.2 M Ω ·cm) from a Millipore-MilliQ system (Molsheim, France) was used for preparing all aqueous solutions.

2.2. Apparatus

The electrochemical measurements were performed with a GCE modified with the MWCNT-IgG nanohybrid, using a platinum wire as an auxiliary electrode, and a Ag/AgCl (3.0 M NaCl) (BASi, West Lafayette, IN, USA) as the reference electrode. All potentials are referred to this electrode. Electrochemical impedance spectroscopy (EIS) experiments were carried out with a PGSTAT30 potentiostat (Metrohm, Herisau, Switzerland) using 1.0×10^{-3} M HQ/BQ (prepared in 0.050 M phosphate buffer pH 7.40) as a redox marker, with the following experimental conditions: amplitude: 0.010 V, range of frequencies: 1.0×10^{-2} to 1.0×10^6 Hz, and working potential: 0.050 V. In the Nyquist plots, the symbols correspond to the experimental points while the solid lines represent the fitting with the model obtained with the Zview program. Voltammetric experiments were performed with a TEQ_04 potentiostat (nanoTeq, Buenos Aires, Argentina).

A TB04TA ultrasonic cleaner (Testlab, Bernal, Argentina) was used for sonication at 40 kHz frequency and 160 W ultrasonic power.

2.3. Preparation of MWCNT-IgG Hybrid and GCE/MWCNT-IgG Platform

The preparation of MWCNT-IgG was performed according to Mujica et al. [21]. Briefly, 2.5 mg of MWCNTs were mixed with 1.0 mL of 2.0 mg mL⁻¹ IgG aqueous solution, and the resulting mixture was sonicated in an ultrasonic bath for 15 min.

GCEs were polished with alumina slurries of 1.0, 0.3, and 0.05 μm for 2.0 min each, rinsed with deionized water and dried with a nitrogen stream. The modification of the polished GCEs with the nanohybrid was carried out by deposition of 10 μL MWCNT-IgG and further solvent evaporation at room temperature (GCE/MWCNT-IgG).

2.4. Construction of the Genosensor (GCE/MWCNT-IgG/DNAP)

First, 10 μL of 150 ppm DNAP were dropped on top of GCE/MWCNT-IgG to obtain the BRCA1 genosensing platform. After drying, the surface was washed with 0.050 M phosphate buffer pH 7.40 and blocked with 2.0% *w/v* BSA for 20 min to avoid non-specific adsorptions (GCE/MWCNT-IgG/DNAP/BSA). Once rinsed with the phosphate buffer, the genosensor was ready to use. The hybridization was performed by dropping 20 μL of the target solution on the top of the nanohybrid-modified GCE for 60 min at room temperature.

Before EIS measuring, the electrode containing the double helix was washed with 0.050 M phosphate buffer pH 7.40 + 0.500 M NaCl (Figure 1).

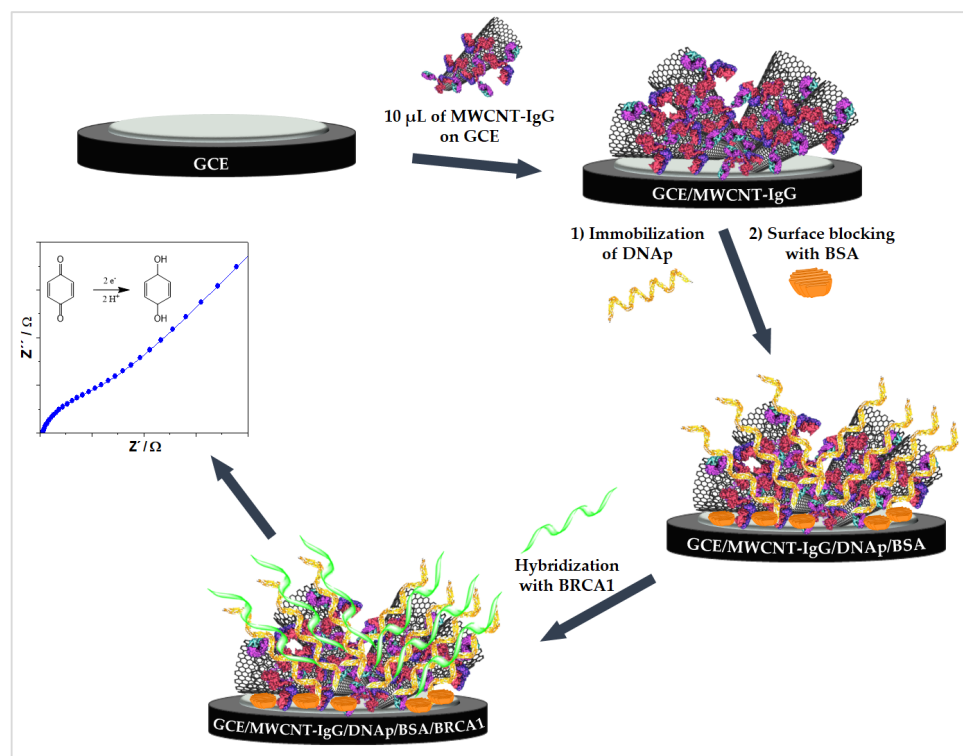


Figure 1. Schematic representation of the construction of the impedimetric genosensor for the quantification of BRCA1 based on the MWCNT-IgG nano hybrid.

2.5. Voltammetric Detection of Do and UA

Linear sweep voltammetry (LSV) was used to quantify Do and UA in the presence of 1.0×10^{-3} M AA. The potential was scanned between -0.300 and 0.500 V at 0.050 V s $^{-1}$.

3. Results and Discussion

3.1. Electrooxidation of the DNA Probe at GCE/MWCNT-IgG

Figure 2 shows linear scan voltammograms obtained in 0.050 M phosphate buffer pH 7.40 at bare GCE (black line) and GCE/MWCNT-IgG (red line) modified by deposition of 150 ppm DNAP until dryness. At bare GCE, the guanine oxidation occurs at 1.024 V, while the adenine oxidation takes place at 1.238 V [57]. On the contrary, at GCE/MWCNT-IgG, there is a considerable decrease in the overvoltages for guanine (160 mV) and adenine (116 mV) electro-oxidation and a large increase in the associated currents (~ 2.8 times for both G and A). This important decrease in the overvoltages is attributed to the catalytic activity of the exfoliated MWCNTs and the favorable electrostatic interaction between the negatively charged sugar-phosphate backbone of the DNAP and the positively charged amino acid residues (lysine, arginine, and histidine) of the IgG (isoelectric point: 7.60–9.34), that facilitates the adsorption and further electrooxidation of the nucleic acid. We also evaluated the electrooxidation of other nucleic acids at the MWCNT-IgG nano hybrid modified GCE like salmon sperm double-stranded DNA, polyguanine, and polyadenine, and in all cases, there was an important decrease in the overvoltages for the oxidation of the electroactive bases. These results demonstrate the advantages of the biofunctionalization of MWCNTs with human IgG for the electrooxidation of nucleic acids, making possible their sensitive detection at the electrode surface at considerably lower potentials. It is important to mention that the platform used for the immobilization of the DNAP was stable since electrodes stored at 4 °C for 3, 7, and 10 days showed responses that correspond to 95, 91, and 86% of the original one, respectively.

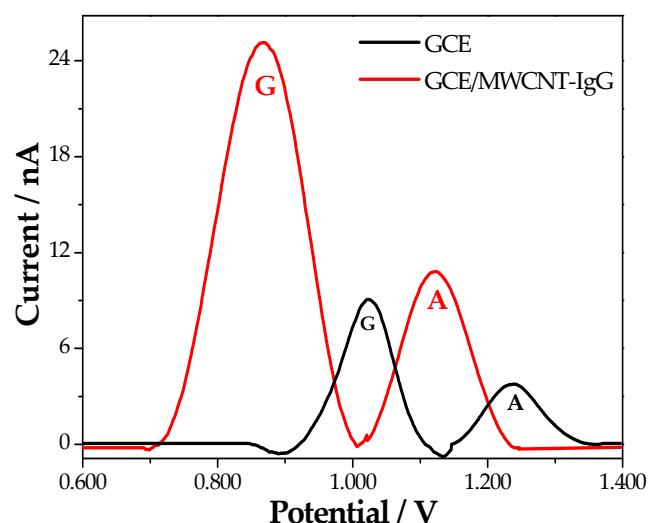


Figure 2. Linear scan voltammograms obtained for immobilization of 150 ppm DNAp on GCE (—) and GCE/MWCNT-IgG (—). G: guanine; A: adenine. Scan rate: 0.050 V s^{-1} . Supporting electrolyte: 0.050 M phosphate buffer pH 7.40.

3.2. Construction of BRCA1 Gene Biosensor and Analytical Applications

Electrochemical Impedance Spectroscopy is a powerful tool for the detection of bioaffinity events at the surface of modified electrodes. In fact, when a biomolecule of high molecular weight binds to an electrode surface by bioaffinity recognition, disturbs the charge transfer kinetics of a redox probe. Figure 3 displays Nyquist plots obtained at GCE/MWCNT-IgG/DNAP blocked with BSA before (red color) and after (blue color) the interaction with $1.0 \times 10^{-12} \text{ M}$ BRCA1. The inset displays the Randles circuit, which was used to fit the experimental results. In this circuit, R_s is the resistance of the solution, R_{CT} is the charge transfer resistance of the redox marker, C_{dl} is the double-layer capacitance and W is the impedance of Warburg. The bars plot for the R_{CT} of the HQ/BQ redox marker obtained at the different surfaces is also shown in the inset. An increase in R_{CT} is obtained once the BRCA1 target interacts with GCE/MWCNT-IgG/DNAP/BSA (796Ω versus 1296Ω , respectively), which is due to the duplex formation resulting in a blockage of the surface.

The effect of the hybridization time at GCE/MWCNT-IgG/DNAP/BSA was evaluated from the changes in R_{CT} of the redox marker in the presence of $1.0 \times 10^{-12} \text{ M}$ BRCA1. As the hybridization time increases, the R_{CT} also increases up to 60 min due to the formation of higher amounts of double helix DNA with the consequent blockage of the surface and lower charge transfer rate. Longer times do not result in an additional increment in R_{CT} due to the saturation of the DNAP available for hybridization. Therefore, 60 min was selected as the optimum.

Figure 4a depicts the Nyquist diagrams obtained for GCE/MWCNT-IgG/DNAP/BSA in the presence of different concentrations of BRCA1 from $1.0 \times 10^{-15} \text{ M}$ to $1.0 \times 10^{-10} \text{ M}$ (1 fM–100 pM). Figure 4b displays the corresponding calibration plot, obtained from the Nyquist plots shown in Figure 4a. There is a linear dependence between R_{CT} and the logarithm of target concentration in the whole range of concentrations evaluated with a sensitivity of $(3.0 \pm 0.1) \times 10^2 \Omega \text{ M}^{-1}$ ($R^2 = 0.9990$) and a detection limit of 0.3 fM (calculated as $3 \times$ standard deviation of the blank signal/sensitivity). The reproducibility was 4.0% for $1.0 \times 10^{-12} \text{ M}$ BRCA1 using five genosensors prepared with the same MWCNT-IgG nanohybrid.

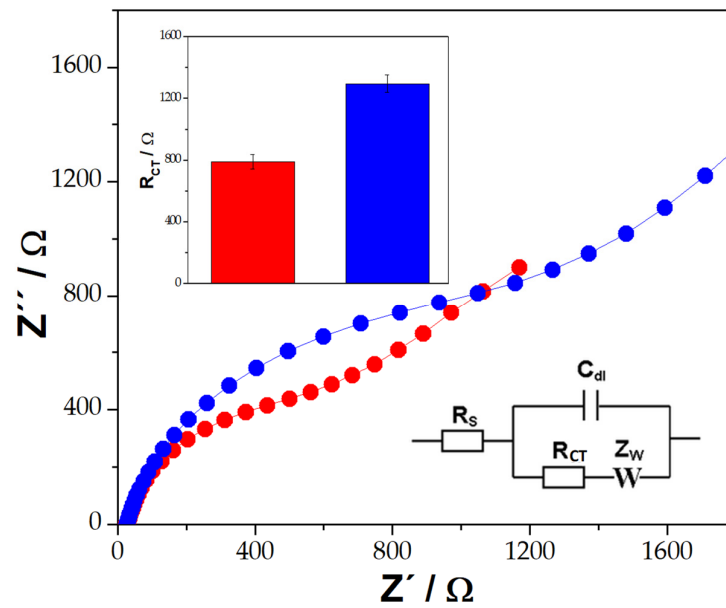


Figure 3. Nyquist plots obtained for GCE/MWCNT-IgG/DNAp/BSA (●) and GCE/MWCNT-IgG/DNAp/BSA/BRCA1 (●). Inset: Bar plots corresponding to the R_{CT} obtained from Nyquist plots. Hybridization time: 60 min. Redox probe: 1.0×10^{-3} M HQ/BQ. Frequency range: 1.0×10^{-2} – 1.0×10^6 Hz; amplitude: 0.010 V; working potential: 0.050 V. Supporting electrolyte: 0.050 M phosphate buffer pH 7.40.

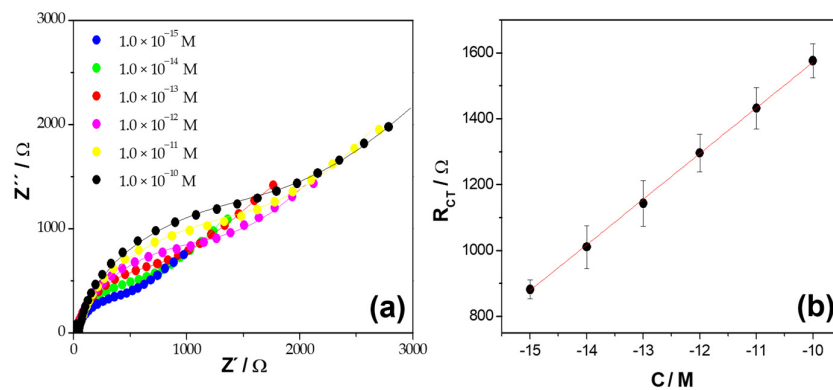


Figure 4. (a) Nyquist plots obtained at GCE/MWCNT-IgG/DNAp/BSA for different concentrations of BRCA1. (b) Calibration plot obtained from Nyquist plots shown in (a). Other conditions as in Figure 3.

Table 1 shows the R_{CT} of the redox marker obtained at GCE/MWCNT-IgG/DNAp/BSA before and after the interaction with 1.0×10^{-12} M BRCA1, 1.0×10^{-12} M NC, 1.0×10^{-12} M Mi, and 1/100 diluted human blood serum without and with 1.0×10^{-12} M BRCA1. In the presence of NC and Mi, there is almost no change in R_{CT} compared to the one obtained at GCE/MWCNT-IgG/DNAp/BSA, evidencing the good selectivity of the biosensing event. Almost no matrix effect was observed for reconstituted human blood serum diluted with 0.050 M phosphate buffer solution + 0.500 M NaCl, while the response for the same serum sample enriched with 1.0×10^{-12} M BRCA1 was 93.8% of the one obtained in the presence of pure target solution. These results indicate that the proposed biosensing platform is highly promising for further practical applications.

Table 1. Selectivity study and proof-of-concept for the analytical application of the GCE/MWCNT-IgG/DNAp genosensor.

Platform	R_{CT}/Ω
GCE/MWCNT-IgG/BSA	$(8.1 \pm 0.2) \times 10^2$
GCE/MWCNT-IgG/BSA/BRCA1 (1.0×10^{-12} M)	$(1.3 \pm 0.5) \times 10^3$
GCE/MWCNT-IgG/BSA/NC (1.0×10^{-12} M)	$(7.9 \pm 0.5) \times 10^2$
GCE/MWCNT-IgG/BSA/Mi (1.0×10^{-12} M)	$(8.1 \pm 0.3) \times 10^2$
GCE/MWCNT-IgG/BSA/Diluted serum 1/100	$(8.0 \pm 0.4) \times 10^2$
GCE/MWCNT-IgG/BSA/Diluted serum 1/100 + BRCA1 (1.0×10^{-12} M)	$(1.22 \pm 0.09) \times 10^3$

Table 2 summarizes the analytical performance of the most relevant BRCA1 electrochemical biosensors reported in the last years. As can be seen, GCE/MWCNT-IgG/DNAp presents a very competitive analytical performance, with a lower detection limit [29–35] or comparable [36,37] than those shown in the table. Wang et al. [29] proposed a differential pulse voltammetric (DPV) biosensor based on a nanocomposite of the conductive polymer poly(3,4-ethylenedioxythiophene) (PEDOT) and a novel antifouling polypeptide (PEP) electrodeposited on the surface of a GCE. PEP acted both as an inhibitor of non-specific protein adsorption and as a binder of the DNAp. Methylene blue (MB) was used as a redox indicator and the concentration of BRCA1 was obtained from the changes in its DPV currents produced as a consequence of the DNAp-BRCA1 hybridization, allowing a detection limit of 3.4 fM. Senel et al. [30] presented another DPV biosensor for the BRCA1 detection using Au electrodes modified with ferrocene (Fc)-cored poly(amidoamine) dendrimers (PAMAM) as support for DNAp, where Fc is a redox marker, and glutaraldehyde works as a linker between PAMAM and DNAp. After a hybridization time of 60 min with the BRCA1 target, Au/Fc-PAMAM/DNAp showed a wide linear range (1.3–20 nM) but a high detection limit (0.38 nM). A graphene oxide (GO) and ionic liquid (IL) composite-modified pencil graphite electrode (PGE) was developed by Işın et al. [31] as an electrochemical platform for BRCA1 quantification. After solution-phase hybridization, the DNAp-BRCA1 hybrids were immobilized on the PGE-GO-IL surface and monitored through the direct measurement of the guanine oxidation signal by DPV, obtaining a detection limit value of $1.48 \mu\text{g mL}^{-1}$ (~6.7 nM). Another strategy for BRCA1 quantification was proposed by using a carbon paste electrode (CPE) modified with electrospinning ribbon conductive nanofibers of poly(ethersulfone) and MWCNTs as a platform for the immobilization of the DNAp and EIS to transduce the hybridization event. Ehzari et al. [32] reported that the EIS signals were proportional to the BRCA1 concentration up to 14 nM with a detection limit of 2.4 pM. An improved detection limit (0.57 fM) was reported by Ehzari et al. [33] using an electrochemical biosensor with a sandwich-type hybridization scheme based on (i) MWCNTs and a core-shell structured magnetic imine-containing metal-organic framework (MOF) (MWCNT/Fe₃O₄@MOF), and (ii) two distinct DNAs, DNAp and ferrocene-functionalized reporter DNA (Fc-DNAr), capable of simultaneously binding to BRCA1. MWCNT/Fe₃O₄@MOF allowed the improvement in the electron transfer between the electroactive species and the electrode and the consequent enhancement of the DPV output signal by redox recycling of the (Fe(CN)₆^{4-/3-}) species. García-Mendiola et al. [34] developed a sensor based on the deposition of a few layers of antimonene on Au screen-printed electrodes and further non-covalent functionalization of antimonene with DNAp to develop a specific BRCA1 sensor. The analytical signal was obtained from the DPV signal of thionine (as a redox indicator) accumulated at the immobilized DNAp before and after hybridization with BRCA1. The detection limit of this genosensor was found to be $28.3 \text{ pg } \mu\text{L}^{-1}$ (~128 pM). Li et al. [35] reported a “signal on-off-off” amplification strategy for the electrochemical detection of the BRCA1 gene. For this, a stem-loop DNAp modified at 5'-end with a thiol group and at 3'-end with MB, was self-assembled on an electrodeposited nanoAu surface, which strengthened the MB electrochemical signal and indicated “signal

on". Then, the BRCA1-DNAp hybridization made MB away from the nanoAu surface and reduced its signal, indicating "signal off". Finally, a further decrease of MB signal was recorded using a duplex-specific nuclease to cleave the DNAp-BRCA1 hybrid, which also indicated the "signal off". Despite the amplification strategy, this genosensor shows a much higher detection limit (52 pM) than our sensor (0.3 fM). Xia et al. [36] obtained a similar detection limit (0.301 fM) to ours with a label-free biosensor based on three-dimensional reduced graphene oxide (3D-rGO) and polyaniline (PANI) nanofibers assembled on the GCE surface. The DNAp for BRCA1 was immobilized to GCE/3D-rGO-PANI via the formation of phosphoramidate bonds between its phosphate group at 5'-end and the amino group of PANI. After hybridization, the analytical signal was obtained from the DPV response of MB embedded into the duplex DNA. A linear range between 1.0 fM and 10.0 pM and a detection limit of 0.3 fM for BRCA1 was reported by Cui et al. [37]. They developed an impedimetric genosensor by applying a self-assembled monolayer of zwitterionic peptides to covalently bind DNAp and prevent non-specific adsorption on the sensing surface (antifouling ability).

Table 2. Comparison of the analytical characteristics of electrochemical biosensors for BRCA1.

Platform	Detection Limit	Linear Range	Ref.
Electrochemical Technique: DPV			
GCE modified with an electrodeposited nanocomposite of PEP-doped PEDOT	3.4 fM	0.01 pM to 1.0 nM	[29]
Au modified with Fc-cored PAMAM as support for DNAp	0.38 nM	1.3 nM to 20 nM	[30]
PGE modified with a GO and IL composite	6.7 nM	---	[31]
AuSPE modified with antimonene non-covalently functionalized with DNAp	28.3 pg μL^{-1} (~128 pM)	0.1 to 20.0 ng μL^{-1} (~452 pM to ~90 nM)	[34]
Electrodeposited nanoAu surface as support for a stem-loop DNAp modified with a thiol group (5'-end) and MB (3'-end)	52 pM	5.0 nM to 70 nM	[35]
GCE modified with 3D-rGO and PANI nanofibers	0.301 fM	1.0 fM to 100 nM	[36]
Electrochemical Technique: EIS			
CPE modified with electrospun conductive nanofibers of PES and MWCNTs as platform to immobilize DNAp	2.4 pM	5.0 pM to 14 nM	[32]
GCE modified with MWCNTs and MOF with Fe_3O_4 nanoparticles core to immobilize DNAp	0.57 fM	1.0 fM to 100 pM	[33]
Au modified with an antifouling zwitterionic peptide SAM to covalently bind DNAp	0.3 fM	1.0 fM to 10.0 pM	[37]
Au modified with MXene/AuNP@BLM to immobilize SH-DNAp	1.0 zM	1.0 zM to 1.0 μM	[38]
GCE modified with rGO and PANHS to graft DNAp	0.35 aM	1.0 aM to 100 pM	[39]
GCE modified with ePDA/TA/tetraPEG/eAuNP to immobilize SH-DNAp	0.05 fM	0.1 fM to 10 pM	[40]
GCE modified with MWCNT-IgG/DNAp	0.3 fM	1.0 fM to 100 pM	This work

Abbreviations: DPV: differential pulse voltammetry; GCE: glassy carbon electrode; PEP: antifouling polypeptide; PEDOT: poly(3,4-ethylenedioxythiophene); Au: gold electrode; Fc: ferrocene; PAMAM: poly(amidoamine) dendrimers; DNAp: deoxyribonucleic acid probe; PGE: pencil graphite electrode; GO: graphene oxide; IL: ionic liquid; AuSPE: gold screen-printed electrode; MB: methylene blue; rGO: reduced graphene oxide; PANI: poly(aniline); EIS: electrochemical impedance spectroscopy; CPE: carbon paste electrode; PES: poly(ethersulfone); MWCNTs: multi-walled carbon nanotubes; MOF: metal-organic framework; SAM: self-assembled monolayer; AuNP: gold nanoparticles; BLM: biomimetic bilayer lipid membrane; SH-DNAp: thiolated deoxyribonucleic acid probe; PANHS: 1-pyrenebutyric acid-N-hydroxysuccinimide; ePDA: electropolymerized poly(dopamine); TA: tannic acid; tetraPEG: four-armed poly(ethylene glycol); eAuNP: electrodeposited gold nanoparticles.

The use of MXene modified with a AuNPs decorated-biomimetic bilayer lipid membrane (AuNP@BLM) [38], rGO or MWCNTs modified with 1-pyrenebutyric acid-N-hydroxysuccinimide (PANHS) [39], and a hydrophilic material based on electropolymerized poly(dopamine), tannic acid (TA), and four-armed poly(ethylene glycol) (ePDA/TA/tetraPEG) with electrodeposited AuNPs [40], presented better detection limits than our biosensor. Divya et al. [38] reported the construction of a label-free electrochemical genosensor based on the synergistic combination of AuNP@BLM with 2D MXene nanosheets and the use of SH-DNAp that allowed an expanded linear range from 10 zM to 1 μ M with a detection limit as low as 1 zM. Benvidi et al. [39] proposed the impedimetric detection of BRCA1 via GCEs modified with rGO and MWCNTs, using PANHS as a suitable base to graft DNAp on the electrode surface and Tween to remove its non-specific adsorption. EIS responses for different concentrations of BRCA1 at GCE/rGO/PANHS/DNAp or GCE/MWCNT/PANHS/DNAp showed a wide linear range that made possible its detection at levels from 0.35 to 3.1 aM, respectively. In addition, Chen et al. [40] fabricated an electrochemical biosensor for BRCA1 quantification by modifying the GCE surface with ePDA/TA/tetraPEG using the layer-by-layer technique. After electrodeposition of AuNPs and immobilization of SH-DNAp on GCE/ePDA/TA/tetraPEG/AuNP, the hybridization experiments were performed by immersing the resulting sensor into different target concentrations (0.1 fM–10 pM), allowing BRCA1 to be detected by EIS with a detection limit of 0.05 fM. This comparison allows us to conclude that our biosensor is competitive since, even when the biosensors reported in [37–39] present better detection limits, they involve more than one nanomaterial associated with lipid membranes, linkers, or polymers, at variance with our BRCA1 genosensor which only contains MWCNTs and IgG.

3.3. Simultaneous Detection of Do and UA in the Presence of AA

The voltammetric response of a mixture of 1.0×10^{-3} M AA, 1.0×10^{-3} M Do, and 1.0×10^{-3} M UA obtained at bare GCE is displayed in the inset of Figure 5. Under these conditions, it is not possible to distinguish the three processes due to the proximity of the oxidation peak potentials. At variance with this behavior (Figure 5), due to the catalytic activity of the efficiently exfoliated MWCNTs, three very well-defined oxidation current peaks are observed in the linear scan voltammogram obtained at GCE modified with MWCNT-IgG for a mixture containing 5.0×10^{-4} M of Do, UA and AA at -0.013 V, 0.147 V, and 0.272 V, for AA, Do and UA, respectively.

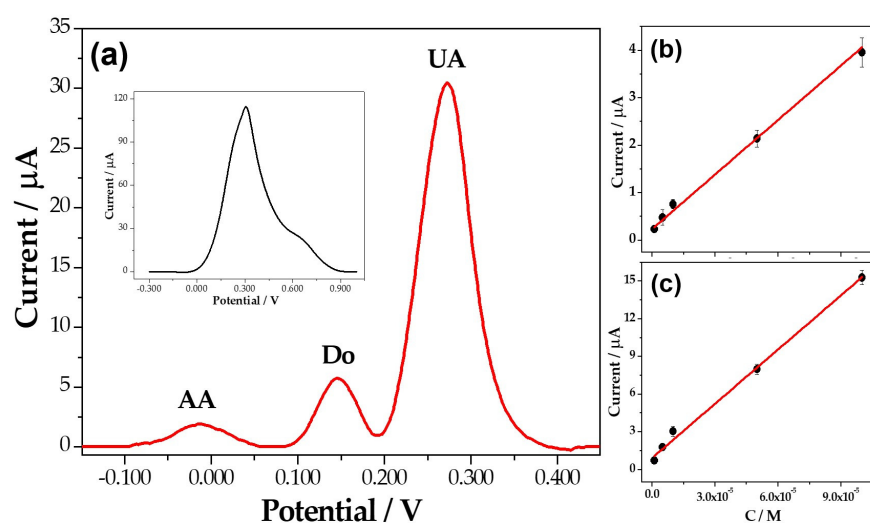


Figure 5. (a) Linear scan voltammogram for 5.0×10^{-4} M Do and 5.0×10^{-4} M UA in presence of 5.0×10^{-4} M AA at GCE/MWCNT-IgG. Inset: Linear scan voltammogram for a mixture of 1.0×10^{-3} M AA, 1.0×10^{-3} M Do, and 1.0×10^{-3} M UA at bare GCE. (b) Calibration plot for Do obtained from LSV recordings. (c) Calibration plot for UA obtained from LSV recordings. Other conditions as in Figure 2.

Based on the different electrochemical behavior of AA, Do, and UA at the surface of GCE/MWCNT-IgG, this sensor allowed us the simultaneous quantification of Do and UA in the presence of AA. As can be seen in Figure 5b,c, there was a linear relationship between 1.0×10^{-6} M and 5.0×10^{-4} M and detection limits of $0.3 \mu\text{M}$ for both analytes, with sensitivities of $(3.8 \pm 0.2) \times 10^4 \mu\text{A M}^{-1}$ ($R^2 = 0.985$) and $(1.44 \pm 0.05) \times 10^5 \mu\text{A M}^{-1}$ ($R^2 = 0.990$) for Do and UA, respectively. Therefore, the successful exfoliation of MWCNTs with IgG allows the development of a very active electrochemical platform that makes possible the resolution of complex mixtures like Do, UA, and AA.

Table 3 compares the analytical characteristics of our sensor with those electrochemical sensors based on CNTs for the simultaneous quantification of Do and UA published since 2021 [58–67]. Among them, Liao et al. [60] reported detection limits for Do and UA comparable and higher to our sensor, respectively; Rattanaumpa et al. [63] presented detection limits higher and comparable than our sensor for Do and UA, respectively, while Li et al. [66] reported comparable detection limits to our sensor for both compounds. The rest of the sensors included in the table [58,59,61,62,64,65,67], allowed the detection of lower levels of Do and UA than the sensor proposed here. However, it is important to remark that in all these cases, at variance with our sensing platform, these sensors involve not only CNTs, but also metal [58] and covalent [62,64,67] organic frameworks; a graphenaceous material [62], polymers like poly(melamine) [59], cyclodextrin, and polyoxometalate [62], making the preparation of the sensor more complex and time-consuming. Therefore, our sensor, which only involves MWCNTs dispersed in IgG, represents a very competitive alternative for the simultaneous quantification of Do and UA in a simple, fast, and label-free way, without any amplification scheme.

Table 3. Comparison of detection limits and linear ranges for Do and UA obtained with GCE/MWCNT-IgG and different CNT-modified GCE.

Platform	Detection Limit (μM)		Linear Range (μM)		Ref.
	Do	UA	Do	UA	
Electrochemical Technique: DPV					
GCE modified with MWCNTs and a Zr-based MOF (DUT-67) grown on ZnCo_2O_4 nanoflowers	0.012	0.0087	1.0 to 180.0	1.0 to 180.0	[58]
GCE modified with a cMWCNT/CD-PMEL nanocomposite obtained by polymerization of CD-fixed MEL residues	0.023	0.064	0.1 to 10	0.1 to 200	[59]
GCE modified with FeNPs encapsulated in BNC	0.8	0.28	1 to 630	0.5 to 2065	[60]
GCE modified with cMWCNTs and TFPB-TAPB-COF	0.073	0.063	0.6 to 250	0.6 to 250	[61]
GCE modified with a rGO- β -CD-cMWCNT-rPOM tetracomponent hybrid	0.04	0.05	0.5 to 300	1 to 400	[62]
GCE modified with microporous carbon	0.2	1.7	10 to 150	10 to 150	[63]
GCE modified with DBTA-TAPT-COF, La_2O_3 , and cMWCNTs	0.039	0.024	2 to 450	0.4 to 450	[64]
GCE modified with a LaV-MWCNT nanocomposite	0.046	0.025	2 to 100	2 to 100	[65]
GCE modified with Gr, SWCNTs, eCeNPs, eCuNPs, and Tween 20	0.0072	0.0063	0.1 to 100	0.08 to 100	[66]
GCE modified with eAuNPs and a TFPPy-PDA-COF— α -MWCNT dispersion	0.21	0.29	0.7 to 108	0.97 to 200	[67]
Electrochemical Technique: LSV					
GCE modified with MWCNT-IgG	0.33	0.33	1 to 500	1 to 500	This work

Abbreviations: DPV: differential pulse voltammetry; GCE: glassy carbon electrode; PEP: antifouling polypeptide; PEDOT: poly(3,4-ethylenedioxythiophene); Au: gold electrode; Fc: ferrocene; PAMAM: poly(amidoamine) dendrimers; DNaP: deoxyribonucleic acid probe; PGE: pencil graphite electrode; GO: graphene oxide; IL: ionic liquid; AuSPE: gold screen-printed electrode; MB: methylene blue; rGO: reduced graphene oxide; PANI: poly(aniline); CPE: carbon paste electrode; PES: poly(ethersulfone); MWCNTs: multi-walled carbon nanotubes; MOF: metal-organic framework; SAM: self-assembled monolayer; AuNP: gold nanoparticles; BLM: biomimetic bilayer lipid membrane; SH-DNaP: thiolated deoxyribonucleic acid probe; PANHS: 1-pyrenebutyric acid-N-hydroxysuccinimide; ePDA: electropolymerized poly(dopamine); TA: tannic acid; tetraPEG: four-armed poly(ethylene glycol); eAuNP: electrodeposited gold nanoparticles; LSV: linear sweep voltammetry.

4. Conclusions

The results presented here demonstrate the advantages of using GCEs with MWCNTs non-covalently biofunctionalized with IgG for the development of two electrochemical sensors. One of them is for the highly sensitive and selective impedimetric quantification of BRCA1 due to the facilitated adsorption of the DNAP at the resulting GCE/MWCNTs-IgG, demonstrating that the interaction of DNAP with MWCNT-IgG does not affect in a significant way the recognition properties of the DNAP. The other one was focused on the voltammetric quantification of Do and UA in the presence of AA, due to the electrocatalytic activity of the exfoliated MWCNTs.

Author Contributions: Conceptualization, P.D. and G.R.; methodology, M.L.M. and A.T.; validation, P.D. and G.R.; formal analysis, M.L.M. and A.T.; investigation, M.L.M. and A.T.; resources, G.R.; writing—original draft preparation, G.R.; writing—review and editing, P.D. and G.R.; visualization, M.L.M. and A.T.; supervision, P.D. and G.R.; funding acquisition, P.D. and G.R. All authors have read and agreed to the published version of the manuscript.

Funding: This research was funded by ANPCyT-FONCyT (PICT 2018-03862, PICT 2019-01114), CONICET (PIP 2022), SECyT-UNC (2018-2023), and SCTyP-UTN (PID PAECBCO0008294TC) from Argentina.

Institutional Review Board Statement: Not applicable.

Informed Consent Statement: Not applicable.

Data Availability Statement: Data are contained within the article.

Acknowledgments: The authors thank ANPCyT, CONICET, SECyT-UNC, and SCTyP-UTN for the financial support. M.L.M. and A.T. thank CONICET for the doctoral fellowships. P.D. and G.R. are members of the Research Career of CONICET.

Conflicts of Interest: The authors declare no conflict of interest.

References

1. Ramya, M.; Senthil, P.; Rangasamy, G.; Saravanan, A.; Krishnapandi, A. A recent advancement on the applications of nanomaterials in electrochemical sensors and biosensors. *Chemosphere* **2022**, *308*, 136416. [[CrossRef](#)] [[PubMed](#)]
2. Safari, M.; Moghaddam, A.; Salehi Moghaddam, A.; Ruckdäschel, H.; Khonakdar, H.A. Carbon-based biosensors from graphene family to carbon dots: A viewpoint in cancer detection. *Talanta* **2023**, *258*, 124399. [[CrossRef](#)] [[PubMed](#)]
3. Song, H.; Liu, Y.; Fang, Y.; Zhang, D. Carbon-based electrochemical sensors for in vivo and in vitro neurotransmitter detection. *Crit. Rev. Anal. Chem.* **2023**, *53*, 955–974. [[CrossRef](#)] [[PubMed](#)]
4. Rathinavel, S.; Priyadharshini, K.; Panda, D. A review on carbon nanotubes: An overview of synthesis, properties, functionalization, characterization, and the application. *Mater. Sci. Eng. B* **2021**, *268*, 115095. [[CrossRef](#)]
5. Palomar, Q.; Xu, X.; Selegård, R.; Aili, D.; Zhang, Z. Peptide decorated gold nanoparticle/carbon nanotube electrochemical sensor for ultrasensitive detection of matrix metalloproteinase-7. *Sens. Actuators B Chem.* **2020**, *325*, 128789. [[CrossRef](#)]
6. Mujica, M.L.; Tamborelli, A.; Castellaro, A.; Barcudi, D.; Rubianes, M.D.; Rodríguez, M.C.; Bocco, J.L.; Dalmaso, P.R.; Rivas, G.A. Impedimetric and amperometric genosensors for the highly sensitive quantification of SARS-CoV-2 nucleic acid using an avidin-functionalized multi-walled carbon nanotubes biocapture platform. *Biosens. Bioelectron. X* **2022**, *12*, 100222. [[CrossRef](#)] [[PubMed](#)]
7. Negahdary, M.; Agnes, L. Application of electrochemical biosensors for the detection of microRNAs (miRNAs) related to cancer. *Coord. Chem. Rev.* **2022**, *464*, 214565. [[CrossRef](#)]
8. Banakar, M.; Hamidi, M.; Khurshid, Z.; Zafar, M.S.; Sapkota, J.; Azizian, R.; Rokaya, D. Electrochemical biosensors for pathogen detection: An updated review. *Biosensors* **2022**, *12*, 927. [[CrossRef](#)]
9. Wu, H.; Zhang, G.; Yang, X. Electrochemical immunosensor based on Fe₃O₄/MWCNTs-COOH/AuNPs nanocomposites for trace liver cancer marker alpha-fetoprotein detection. *Talanta* **2023**, *259*, 124492. [[CrossRef](#)]
10. Peng, Y.; Ou, S.; Li, M.; Zeng, Z.; Feng, N. An electrochemical biosensor based on network-like DNA nanoprobes for detection of mesenchymal circulating tumor cells. *Biosens. Bioelectron.* **2023**, *238*, 115564. [[CrossRef](#)]
11. Mujica, M.L.; Zhang, Y.; Gutiérrez, F.; Bédioui, F.; Rivas, G. Non-amplified impedimetric genosensor for quantification of miRNA-21 based on the use of reduced graphene oxide modified with chitosan. *Microchem. J.* **2021**, *160*, 105596. [[CrossRef](#)]
12. Alosime, E.M. A review on surface functionalization of carbon nanotubes: Methods and applications. *Nanoscale Res. Lett.* **2023**, *18*, 12. [[CrossRef](#)] [[PubMed](#)]
13. Kharlamova, M.V.; Paukov, M.; Burdanova, M.G. Nanotube functionalization: Investigation, methods and demonstrated applications. *Materials* **2022**, *15*, 5386. [[CrossRef](#)] [[PubMed](#)]

14. Zhou, Y.; Fang, Y.; Ramasamy, R.P. Non-covalent functionalization of carbon nanotubes for electrochemical biosensor development. *Sensors* **2019**, *19*, 392. [[CrossRef](#)] [[PubMed](#)]
15. Gutierrez, F.; Rubianes, M.D.; Rivas, G.A. New bioanalytical platform based on the use of avidin for the successful exfoliation of multi-walled carbon nanotubes and the robust anchoring of biomolecules. Application for hydrogen peroxide biosensing. *Anal. Chim. Acta* **2019**, *1065*, 12–20. [[CrossRef](#)] [[PubMed](#)]
16. Eguílaz, M.; Gutierrez, A.; Rivas, A. Non-covalent functionalization of multi-walled carbon nanotubes with cytochrome c: Enhanced direct electron transfer and analytical applications. *Sens. Actuators B Chem.* **2016**, *216*, 629–637. [[CrossRef](#)]
17. Primo, E.N.; Cañete-Rosales, P.; Bollo, S.; Rubianes, M.D.; Rivas, G.A. Dispersion of bamboo type multi-wall carbon nanotubes in calf-thymus double stranded DNA. *Colloids Surf. B* **2013**, *108*, 329–336. [[CrossRef](#)]
18. Ortiz, E.; Gallay, P.; Galicia, L.; Eguílaz, M.; Rivas, G. Nanoarchitectures based on multi-walled carbon nanotubes non-covalently functionalized with Concanavalin A: A new building-block with supramolecular recognition properties for the development of electrochemical biosensors. *Sens. Actuators B Chem.* **2019**, *292*, 254–262. [[CrossRef](#)]
19. Gallay, P.; Eguílaz, M.; Rivas, G. Designing electrochemical interfaces based on nanohybrids of avidin functionalized-carbon nanotubes and ruthenium nanoparticles as peroxidase-like nanozyme with supramolecular recognition properties for site-specific anchoring of biotinylated residues. *Biosens. Bioelectron.* **2020**, *148*, 111764. [[CrossRef](#)]
20. López Mujica, M.; Rubianes, M.D.; Rivas, G. A multipurpose biocapture nanoplatform based on multiwalled-carbon nanotubes non-covalently functionalized with avidin: Analytical applications for the non-amplified and label-free impedimetric quantification of BRCA1. *Sens. Actuators B Chem.* **2022**, *357*, 131304. [[CrossRef](#)]
21. López Mujica, M.; Tamborelli, A.; Espinosa, C.; Vaschetti, V.; Bollo, S.; Dalmasso, P.; Rivas, G. Two birds with one stone: Integrating exfoliation and immunoaffinity properties in multi-walled carbon nanotubes by non-covalent functionalization with human immunoglobulin G. *Microchim. Acta* **2023**, *190*, 73. [[CrossRef](#)] [[PubMed](#)]
22. Edri, E.; Regev, O. “Shaken, not stable”: Dispersion mechanism and dynamics of protein-dispersed nanotubes studied via spectroscopy. *Langmuir* **2009**, *25*, 10459–10465. [[CrossRef](#)] [[PubMed](#)]
23. Nyberg, T.; Tischkowitz, M.; Antoniou, A.C. BRCA1 and BRCA2 pathogenic variants and prostate cancer risk: Systematic review and meta-analysis. *Br. J. Cancer* **2022**, *126*, 1067–1081. [[CrossRef](#)] [[PubMed](#)]
24. Glodzik, D.; Bosch, A.; Hartman, J.; Aine, M.; Vallon-Christersson, J.; Reuterswård, C.; Karlsson, A.; Mitra, S.; Niméus, E.; Holm, K.; et al. Comprehensive molecular comparison of BRCA1 hypermethylated and BRCA1 mutated triple negative breast cancers. *Nat. Commun.* **2020**, *11*, 3747. [[CrossRef](#)] [[PubMed](#)]
25. Madariaga, H.; Lheureux, S.; Oza, A.M. Tailoring ovarian cancer treatment: Implications of BRCA1/2 mutations. *Cancer* **2019**, *11*, 416. [[CrossRef](#)] [[PubMed](#)]
26. Hawsawi, Y.M.; Al-Numair, N.S.; Sobahy, T.M.; Al-Ajmi, A.M.; Al-Harbi, R.M.; Baghdadi, M.A.; Oyouni, A.A.; Alamer, O.M. The role of BRCA1/2 in hereditary and familial breast and ovarian cancers. *Mol. Genet. Genom. Med.* **2019**, *7*, e879. [[CrossRef](#)] [[PubMed](#)]
27. Venkitaraman, A.R. How do mutations affecting the breast cancer genes BRCA1 and BRCA2 cause cancer susceptibility? *DNA Repair* **2019**, *81*, 102668. [[CrossRef](#)]
28. Philpott, S.; Raikou, M.; Manchanda, R.; Lockley, M.; Singh, N.; Scott, M.; Evans, D.G.; Adlard, J.; Ahmed, M.; Edmondson, R.; et al. The avoiding late diagnosis of ovarian cancer (ALDO) project; a pilot national surveillance programme for women with pathogenic germline variants in BRCA1 and BRCA2. *J. Med. Genet.* **2023**, *60*, 440–449. [[CrossRef](#)]
29. Wang, J.; Wang, D.; Hui, N. A low fouling electrochemical biosensor based on the zwitterionic polypeptide doped conducting polymer PEDOT for breast cancer marker BRCA1 detection. *Bioelectrochemistry* **2020**, *136*, 107595. [[CrossRef](#)]
30. Senel, M.; Dervisevic, M.; Kokkokoglu, F. Electrochemical DNA biosensors for label free breast cancer gene marker detection. *Anal. Bioanal. Chem.* **2019**, *411*, 2925–2935. [[CrossRef](#)]
31. Işın, D.; Eksin, E.; Erdem, A. Graphene-oxide and ionic liquid modified electrodes for electrochemical sensing of breast cancer 1 gene. *Biosensors* **2022**, *12*, 95. [[CrossRef](#)] [[PubMed](#)]
32. Ehzari, H.; Safari, M.; Shahlaei, M. A simple and label-free genosensor for BRCA1 related sequence based on electrospun ribbon conductive nanofibers. *Microchem. J.* **2018**, *143*, 118–126. [[CrossRef](#)]
33. Ehzari, H.; Safari, M.; Samini, M. Signal amplification of novel sandwich-type genosensor via catalytic redox-recycling on platform MWCNTs/Fe₃O₄@TMU-21 for BRCA1 gene detection. *Talanta* **2021**, *234*, 122698. [[CrossRef](#)] [[PubMed](#)]
34. García-Mendiola, C.; Gutierrez-Sánchez, C.; Gibaja, I.; Torres, C.; Buso-Rogero, F.; Pariente, J.; Solera, Z.; Razavifar, J.J.; Palacios, F.; Zamora, E.; et al. Functionalization of a few-layer antimonene with oligonucleotides for DNA sensing. *ACS Appl. Nano Mater.* **2020**, *3*, 3625–3633. [[CrossRef](#)]
35. Li, Z.; Cheng, J.; Zhang, L.; Liu, Y.; Jia, Y.; Zhou, G. Signal “on-off-off” strategy for improving the sensitivity of BRCA1 electrochemical detection by combining gold substrate amplification, DNA conformational transformation and DSN enzymatic hydrolysis dual reduction. *Anal. Chim. Acta* **2022**, *1235*, 340461. [[CrossRef](#)]
36. Xia, Y.M.; Li, M.Y.; Chen, C.L.; Xia, M.; Zhang, W.; Gao, W.W. Employing label-free electrochemical biosensor based on 3D-reduced graphene oxide and polyaniline nanofibers for ultrasensitive detection of breast cancer BRCA1 biomarker. *Electroanalysis* **2020**, *32*, 2045–2055. [[CrossRef](#)]
37. Cui, M.; Wang, Y.; Wang, H.; Wua, Y.; Luo, X. A label-free electrochemical DNA biosensor for breast cancer marker BRCA1 based on self-assembled antifouling peptide monolayer. *Sens. Actuators B Chem.* **2017**, *244*, 742–749. [[CrossRef](#)]

38. Divya, K.P.; Keerthana, S.; Viswanathan, C.; Ponpandian, N. MXene supported biomimetic bilayer lipid membrane biosensor for zeptomole detection of BRCA1 gene. *Microchim. Acta* **2023**, *190*, 116. [[CrossRef](#)]
39. Benvidi, A.; Tezerjani, M.D.; Jahanbani, S.; Ardakani, M.M.; Moshtaghiooun, S.M. Comparison of impedimetric detection of DNA hybridization on the various biosensors based on modified glassy carbon electrodes with PANHS and nanomaterials of RGO and MWCNTs. *Talanta* **2016**, *147*, 621–627. [[CrossRef](#)]
40. Chen, L.; Liu, X.; Chen, C. Impedimetric biosensor modified with hydrophilic material of tannic acid/polyethylene glycol and dopamine-assisted deposition for detection of breast cancer-related BRCA1 gene. *J. Electroanal. Chem.* **2017**, *791*, 204–210. [[CrossRef](#)]
41. Lee, J.Y.; Martín-Bastida, A.; Murueta-Goyena, A.; Gabilondo, I.; Cuenca, N.; Piccini, P.; Jean, B. Multimodal brain and retinal imaging of dopaminergic degeneration in Parkinson disease. *Nat. Rev. Neurol.* **2022**, *18*, 203–220. [[CrossRef](#)] [[PubMed](#)]
42. Broome, S.T.; Louangaphay, K.; Keay, K.A.; Leggio, G.A.; Musumeci, G.; Castorina, A. Dopamine: An immune transmitter. *Neural. Regen. Res.* **2020**, *15*, 2173–2185.
43. Gonzalez-Lopez, E.; Vrana, K.E. Dopamine beta-hydroxylase and its genetic variants in human health and disease. *J. Neurochem.* **2020**, *152*, 157–181. [[CrossRef](#)] [[PubMed](#)]
44. Constantinides, V.C.; Souvatzoglou, M.; Paraskevas, G.P.; Chalioti, M.; Stefanis, L.; Kapaki, E. Dopamine transporter SPECT imaging in Parkinson's disease and atypical parkinsonism: A study of 137 patients. *Neurol. Sci.* **2023**, *44*, 1613–1623. [[CrossRef](#)] [[PubMed](#)]
45. Méndez-Salazar, E.O.; Martínez-Nava, G.A. Uric acid extrarenal excretion: The gut microbiome as an evident yet understated factor in gout development. *Rheumatol. Int.* **2022**, *42*, 403–412. [[CrossRef](#)] [[PubMed](#)]
46. Lanaspa, M.A.; Andres-Hernando, A.; Kuwabara, M. Uric acid and hypertension. *Hypertens. Res.* **2020**, *43*, 832–834. [[CrossRef](#)]
47. Saito, Y.; Tanaka, A.; Node, K.; Kobayashi, Y. Uric acid and cardiovascular disease: A clinical review. *J. Cardiol.* **2021**, *78*, 51–57. [[CrossRef](#)]
48. Przewodowska, D.; Marzec, W.; Madetko, N. Novel therapies for parkinsonian syndromes-Recent progress and future perspectives. *Front. Mol. Neurosci.* **2021**, *14*, 720220. [[CrossRef](#)]
49. Murugan, N.; Jerome, R.; Preethika, M.; Sundaramurthy, A.; Sundramoorthy, A.K. 2D-titanium carbide (MXene) based selective electrochemical sensor for simultaneous detection of ascorbic acid, dopamine and uric acid. *J. Mater. Sci. Technol.* **2021**, *72*, 122–131. [[CrossRef](#)]
50. Li, M.; Xu, H.; Chen, G.; Sun, S.; Wang, Q.; Liu, B.; Wu, X.; Zhou, L.; Chai, Z.; Sun, X.; et al. Impaired D2 receptor-dependent dopaminergic transmission in prefrontal cortex of awake mouse model of Parkinson's disease. *Brain* **2019**, *142*, 3099–3115. [[CrossRef](#)]
51. Xie, X.; Wang, D.P.; Guo, C.; Liu, Y.; Rao, Q.; Lou, F.; Li, Q.; Dong, Y.; Li, Q.; Yang, H.B.; et al. Single-atom ruthenium biomimetic enzyme for simultaneous electrochemical detection of dopamine and uric acid. *Anal. Chem.* **2021**, *93*, 4916–4923. [[CrossRef](#)] [[PubMed](#)]
52. Tchekep, A.G.K.; Suryanarayanan, V.; Pattanayak, D.K. Alternative approach for highly sensitive and free-interference electrochemical dopamine sensing. *Carbon* **2023**, *204*, 57–69. [[CrossRef](#)]
53. Pan, J.; Liu, M.; Li, D.; Zheng, H.; Zhang, D. Overoxidized poly(3, 4-ethylenedioxythiophene)-gold nanoparticles-graphene-modified electrode for the simultaneous detection of dopamine and uric acid in the presence of ascorbic acid. *J. Pharm. Anal.* **2021**, *11*, 699–708. [[CrossRef](#)] [[PubMed](#)]
54. Yang, N.; Chen, X.; Ren, T.; Zhang, P.; Yang, D. Carbon nanotube based biosensors. *Sens. Actuators B Chem.* **2015**, *207*, 690–715. [[CrossRef](#)]
55. Dai, B.; Zhou, R.; Ping, J.; Ying, Y.; Xie, L. Recent advances in carbon nanotube-based biosensors for biomolecular detection. *Trends Anal. Chem.* **2022**, *154*, 116658. [[CrossRef](#)]
56. Burns, G.; Ali, M.Y.; Howlader, M.M.R. Advanced functional materials for electrochemical dopamine sensors. *Trends Anal. Chem.* **2023**, *169*, 117367. [[CrossRef](#)]
57. Olivera-Brett, A.M.; Dicolescu, V.; Piedade, J.V.A. Electrochemical oxidation mechanism of guanine and adenine using a glassy carbon microelectrode. *Bioelectrochemistry* **2022**, *154*, 61–62. [[CrossRef](#)]
58. Wei, X.; Guo, H.; Lu, Z.; Sun, L.; Pan, Z.; Liu, B.; Peng, L.; Yang, W. A novel electrochemical sensor based on DUT-67/ZnCo₂O₄-MWCNTs modified glassy carbon electrode for the simultaneous sensitive detection of dopamine and uric acid. *Colloids Surf. A* **2023**, *674*, 131921. [[CrossRef](#)]
59. Zhou, X.; Kuang, Y.; Li, J.; Hu, S.; Cheng, C.; Wang, J.; Qin, X.; Ou, L.; Su, Z. Melamine-based nanocomposites for selective dopamine and uric acid sensing. *ACS Appl. Polym. Mater.* **2023**, *5*, 5609–5619. [[CrossRef](#)]
60. Liao, Y.; Liu, J.; Liu, M.; Lin, L.; Wang, X.; Quan, Z. Iron nanoparticles encapsulated in boron-nitrogen co-doped carbon nanotubes biomimetic enzyme for electrochemical monitoring of dopamine and uric acid in human serum. *Microchem. J.* **2023**, *185*, 108184. [[CrossRef](#)]
61. Guo, H.; Liu, B.; Pan, Z.; Sun, L.; Peng, L.; Chen, Y.; Wu, N.; Wang, M.; Yang, W. Electrochemical determination of dopamine and uric acid with covalent organic frameworks and ox-MWCNT co-modified glassy carbon electrode. *Colloids Surf. A* **2022**, *648*, 129316. [[CrossRef](#)]

62. Ma, C.; Xu, P.; Chen, H.; Cui, J.; Guo, M.; Zhao, J. An electrochemical sensor based on reduced graphene oxide/ β -cyclodextrin/multiwall carbon nanotubes/polyoxometalate tetracomponent hybrid: Simultaneous determination of ascorbic acid, dopamine and uric acid. *Microchem. J.* **2022**, *180*, 107533. [[CrossRef](#)]
63. Rattanaumpa, T.; Maensiri, S.; Ngamchuea, K. Microporous carbon in the selective electro-oxidation of molecular biomarkers: Uric acid, ascorbic acid, and dopamine. *RSC Adv.* **2022**, *12*, 18709–18721. [[CrossRef](#)] [[PubMed](#)]
64. Pan, Z.; Guo, H.; Sun, L.; Liu, B.; Chen, Y.; Zhang, T.; Wang, M.; Peng, L.; Yang, W. A novel electrochemical platform based on COF/La₂O₃/MWCNTs for simultaneous detection of dopamine and uric acid. *Colloids Surf. A* **2022**, *6350*, 128083. [[CrossRef](#)]
65. You, Y.; Zou, J.; Li, W.-J.; Chen, J.; Jiang, X.-Y.; Yu, J.-G. Novel lanthanum vanadate-based nanocomposite for simultaneously electrochemical detection of dopamine and uric acid in fetal bovine serum. *Int. J. Biol. Macromol.* **2022**, *195*, 346–355. [[CrossRef](#)]
66. Li, R.; Liang, H.; Zhu, M.; Lai, M.; Wang, S.; Zhang, H.; Ye, H.; Zhu, R.; Zhang, W. Electrochemical dual signal sensing platform for the simultaneous determination of dopamine, uric acid and glucose based on copper and cerium bimetallic carbon nanocomposites. *Bioelectrochemistry* **2021**, *139*, 107745. [[CrossRef](#)]
67. Guan, Q.; Guo, H.; Xue, R.; Wang, M.; Zhao, X.; Fan, T.; Yang, W.; Xu, M.; Yang, W. Electrochemical sensor based on covalent organic frameworks-MWCNT-NH₂/AuNPs for simultaneous detection of dopamine and uric acid. *J. Electroanal. Chem.* **2021**, *880*, 114932. [[CrossRef](#)]

Disclaimer/Publisher's Note: The statements, opinions and data contained in all publications are solely those of the individual author(s) and contributor(s) and not of MDPI and/or the editor(s). MDPI and/or the editor(s) disclaim responsibility for any injury to people or property resulting from any ideas, methods, instructions or products referred to in the content.